Global Change Biology

Global Change Biology (2017), doi: 10.1111/gcb.13640

Reconciling seasonal hydraulic risk and plant water use through probabilistic soil–plant dynamics

XUE FENG[1,2], TODD E. DAWSON[3,4], DAVID D. ACKERLY[3], LOUIS S. SANTIAGO[5] and SALLY E. THOMPSON[1]

[1]*Department of Civil and Environmental Engineering, University of California, Berkeley, CA 94720, USA,* [2]*Department of Civil, Environmental, and Geo-Engineering, University of Minnesota, Twin Cities, MN 55455, USA,* [3]*Department of Integrative Biology, University of California, Berkeley, CA 94720, USA,* [4]*Department of Environmental Sciences, Policy, and Management, University of California, Berkeley, CA 94720, USA,* [5]*Department of Botany & Plant Sciences, University of California, Riverside, CA 92521, USA*

Abstract

Current models used for predicting vegetation responses to climate change are often guided by the dichotomous needs to resolve either (i) internal plant water status as a proxy for physiological vulnerability or (ii) external water and carbon fluxes and atmospheric feedbacks. Yet, accurate representation of fluxes does not always equate to accurate predictions of vulnerability. We resolve this discrepancy using a hydrodynamic framework that simultaneously tracks plant water status and water uptake. We couple a minimalist plant hydraulics model with a soil moisture model and, for the first time, translate rainfall variability at multiple timescales – with explicit descriptions at daily, seasonal, and interannual timescales – into a physiologically meaningful metric for the risk of hydraulic failure. The model, parameterized with measured traits from chaparral species native to Southern California, shows that apparently similar transpiration patterns throughout the dry season can emerge from disparate plant water potential trajectories, and vice versa. The parsimonious set of parameters that captures the role of many traits across the soil–plant–atmosphere continuum is then used to establish differences in species sensitivities to shifts in seasonal rainfall statistics, showing that co-occurring species may diverge in their risk of hydraulic failure despite minimal changes to their seasonal water use. The results suggest potential shifts in species composition in this region due to species-specific changes in hydraulic risk. Our process-based approach offers a quantitative framework for understanding species sensitivity across multiple timescales of rainfall variability and provides a promising avenue toward incorporating interactions of temporal variability and physiological mechanisms into drought response models.

Keywords: drought response, plant hydraulic risk, rainfall variability, soil–plant feedback, stochastic soil moisture dynamics

Received 21 November 2016 and accepted 14 January 2017

Introduction

Ecohydrology can make two important and related contributions to the study of global change: (i) the prediction of plant vulnerability to variations in the water cycle and (ii) a description of the water cycle that accounts for the role of vegetation in mediating water fluxes. Access to and utilization of water by plants is the nexus between these issues, for it is the internal water status of individual plants that controls both their water uptake and their experience of physiological stress. Despite this link, contemporary studies of vegetation change and of water cycling are often addressed through different approaches, by different research communities. For example, statistical models are widely used for forecasting changes in species distributions and drought mortality, based on observed correlations between species' performance and climate variables (Araujo & Peterson, 2012). These models rely on stationarity assumptions that may be confounded by changing biotic interactions, land use, or climate, and due to lack of mechanistic foundations, they offer little prognostic insight into ecosystem function. On the other hand, land surface models (LSMs) are used to describe ecosystem carbon and water fluxes, often as boundary conditions to large-scale climate models. LSMs adopt phenomenological relationships between environmental conditions and plant stress, and coarsely resolve these relationships by plant functional type. This approach omits descriptions of either plants' internal water status, or of differences in species-level functional responses, despite the demonstrated influence of species-level characteristics on land surface fluxes (Breshears *et al*., 2009; Knapp *et al*., 2012). While such simplifications are preferred in models that aim to describe landscape scale phenomena, the phenomenological descriptions of stress and the lack of species specificity are implicated in significant failure of LSM

Correspondence: Xue Feng, e-mail: feng@umn.edu

schemes (Powell *et al.*, 2013). Notably, LSMs have limited ability to represent the processes leading to drought mortality and ecosystem reorganization, and exhibit large uncertainties in their prediction of carbon cycling during and after drought (Sitch *et al.*, 2008; Galbraith *et al.*, 2010).

Given the connections between community composition and ecosystem function (Adams *et al.*, 2012), preserving the existing dichotomy between modeling species distribution/drought mortality vs. water and carbon cycling is undesirable. Instead, predictions of species-specific responses to their climatic and edaphic environments – both in terms of the hydraulic status of plants that informs drought vulnerability, and the resulting mediation of water and carbon fluxes – are needed. These predictions can be made using physiologically based models (Sperry *et al.*, 1998; Mackay *et al.*, 2015) that mechanistically describe both plant water status and water fluxes. But to operate at the spatial scales of LSMs, such species-specific frameworks must find the balance between the simplicity that enables large-scale application and the complexity that maximizes process fidelity.

Here, we propose a parsimonious approach to capture species-level responses to varying water availability and atmospheric demand, and explore its ability to simultaneously represent plant water status and plant-mediated water fluxes under seasonal drought conditions. This approach couples a minimalist plant hydraulic model with a probabilistic soil moisture model. By explicitly operating within a probabilistic framework that considers rainfall variability at interannual, seasonal, and daily timescales, we address two interrelated issues: the potentially irreducible uncertainty in rainfall characteristics under climate change scenarios (Hawkins & Sutton, 2011) which calls for risk-based, rather than deterministic, assessment strategies; and the multiscale nature of plants' responses to drought (Katul *et al.*, 2007). In the seasonally dry Mediterranean-type climate that we focus on, plants are sensitive to multiple dimensions of seasonality such as the timing of rainfall at the beginning of the wet season, which triggers leaf flushing, and the wet/dry season lengths, which determine the periods of water availability and scarcity. Rainfall amount and variability in the wet season control the amount of soil water available for plant use in the dry season (Viola *et al.*, 2008). The progressive drydown of soil moisture during the dry season leads to a decrease in plant water status. This decrease is regulated by a suite of physiological traits that can vary among co-existing species (Vico *et al.* 2015). For example, deeper roots allow plants to access additional water sources to buffer the decay in soil moisture (Miller *et al.*, 2010), shedding leaves reduces water demand (Eamus, 1999), and early stomatal closure maintains water potentials above critical physiological thresholds (Tardieu & Simonneau, 1998). Thus, seasonal plant water status arises from a dynamic feedback between seasonal soil water availability and the way in which plants make use of it over time.

The seasonal trajectory of mean soil moisture is described by a probabilistic soil moisture model, based on mass conservation within the hydrologically active soil layer and forced by stochastic daily rainfall (Methods, Supporting Information). The likelihood of rainfall varies between the dry and the wet season, which drives the annual cycle of soil moisture depletion and recharge, as well as from year to year, forming the probabilistic basis for defining the risk of a plant experiencing particular physiological events. The key to the modeling approach lies in establishing a one-to-one correspondence between a plant's hydraulic status (e.g., internal water potentials) and its boundary conditions (e.g., soil moisture and atmospheric vapor pressure deficit), whose temporal trajectories are in turn prescribed by climate and multiscale rainfall statistics. The transpiration to soil moisture relationship for each species emerges from the confluence of climate, soil, and plant properties (e.g., Sperry *et al.*, 2002) rather than being imposed *a priori*, as in many LSMs. Through this process-based dynamic approach, we are able to move beyond a projection of species persistence based on summary climate statistics (e.g., mean annual precipitation) and quantitatively assess species sensitivity to changes in rainfall variability at different timescales. The relative simplicity of the model also enables rapid computation and the ability to make projections at landscape scales.

We parameterize the model using plant traits measured from a diverse set of woody shrub species occurring across a chaparral–desert ecotone in California (Table S1; Pivovaroff *et al.*, 2016), exhibiting a seasonal summer-dry climate. The species are markedly different in their vulnerability to drought-induced physiological stress, as illustrated by the variation in cavitation resistance, represented by the stem water potential corresponding to 50% loss in conductivity ($\psi_{T,50}$), and in their hydraulic safety margins, or the difference between measured seasonal minimum stem water potential ($\psi_{T,min}$) and $\psi_{T,50}$ (Choat *et al.*, 2012; Skelton *et al.*, 2015). Negative margins indicate that plants are routinely operating at a loss of hydraulic conductivity of 50% or more, implying an increased propensity toward hydraulic impairment.

We confirm that the simple modeling framework (i) generates results that are consistent with within-season

time courses of plant water potential and transpiration, and (ii) projects differences in drought susceptibility that are consistent with the range and observed mortality/dieback behavior of two contrasting species. We show that at seasonal scales, divergent physiological states (in terms of plant water potential trajectories) can produce convergent functional outcomes (in terms of transpiration), and vice versa, highlighting the potential pitfalls associated with the dichotomous treatment of water fluxes vs. plant range/drought vulnerability in contemporary modeling approaches. Finally, the model is used to develop a risk-based framework to describe the likelihood of crossing critical hydraulic thresholds in any given year. While defining the critical thresholds for physiological failure remains a challenging area of research (Sevanto *et al.*, 2014), recent evidence has implicated hydraulic failure as a major mode of mortality in woody species (Barigah *et al.*, 2013; Anderegg *et al.*, 2016), with the loss of xylem conductivity quantified by the vulnerability curve (Tyree & Ewers, 1991). With this risk metric, we show that divergent responses to anticipated changes in rainfall seasonality in Southern California will arise at the species level, driven by species-specific physiological traits and their interaction with rainfall variability.

Material and methods

Study site and climate information

The study site is located in Morongo Valley, California, USA (34°02′12″N, 116°37′24″W), in a dry Mediterranean-type climate (Pivovaroff *et al.*, 2016). The vegetation type is representative of an ecotone between chaparral shrublands and Mojave Desert scrub, and the species studied are listed in Table S1. Soils at the site are classified as loamy sand. Table S2 lists soil hydraulic properties with other biome-level soil and vegetation parameters. Climate information, including seasonal rainfall statistics, are extracted from the Global Historical Climatology Network at the daily scale (Menne *et al.*, 2012) at the Twentynine Palms station, based on precipitation measurements from 1960 to 2015. Vapor pressure deficit is calculated from data from the California Irrigation Management Information System (http://www.cimis.water.ca.gov) at the Joshua Tree station. The dry season is designated as being from April to October, while the wet season is from November to March.

Plant hydraulics model

The plant hydraulic model used here comprises a series of flux–gradient relationships spanning the soil–plant–atmosphere continuum. Water flow is driven by a water potential gradient and mediated by checkpoints at the root–soil interface, in the stem, and within the canopy that respond to changing local water status (Fig. 1). The daily equilibrium water flux (E) along the soil–plant–atmosphere continuum can be modeled as a product of a conductivity (or a conductance) and a driving force, with the latter expressed as the water potential gradient between adjacent points in the plant or its environment (Manzoni *et al.*, 2013, 2014). Assuming no storage within the plant at the daily timescale, the mean flux in all components can be equated as:

$$E = g_R(\psi_S)(\psi_S - \psi_T) = g_X(\psi_T)(\psi_T - \psi_L) = g_C(\psi_L)D, \quad (1)$$

where ψ_S, ψ_T, ψ_L are the water potentials in the soil, stem, and leaf, and g_R, g_X, g_C are the soil–root conductivity (m day^{-1} MPa^{-1}), the stem-scale xylem conductivity (m day^{-1} MPa^{-1}), and canopy-scale stomatal conductance (m day^{-1}) as functions of local water potentials, and D is the vapor pressure deficit (mol mol^{-1}).

To capture the decline of g_R, g_X, and g_C in Eqn (1) with respect to local water potentials, we use the following functions (Manzoni *et al.*, 2014):

$$\begin{aligned} g_C(\psi_L) &= \max\left[0, g_{C,\max}\left(1 - \frac{\psi_L}{\psi_{L,0}}\right)\right], \\ g_X(\psi_T) &= g_{X,\max}\left(1 - \frac{1}{1 + e^{a(\psi_T - \psi_{T,50})}}\right) \quad \text{or} \\ g_X(\psi_T) &= g_{X,\max}e^{-m\psi_T}, \\ g_R(\psi_S) &= g_{R,\max}s^{c-d} = g_{R,\max}\left(\frac{\psi_{S,sat}}{\psi_S}\right)^{(c-d)/b}. \end{aligned} \quad (2)$$

The dependence of the stomatal conductance on leaf water potential is modeled as a linear decay, the xylem conductivity based on an exponential sigmoidal (Pammenter & Willigen, 1998) or an exponential function (whichever gives the better fit to data, Fig. 1a; $\psi_{T,50}$ is the water potential at 50% loss in maximum xylem conductivity, a and m are fitting parameters), and the soil–root conductivity a power law decay based on the soil water retention curve where $\psi_S = \psi_{S,sat}s^{-b}$ (Clapp & Hornberger, 1978; Laio *et al.*, 2001), with $c = 2b + 3$ and $d = 4$.

The set of three equations in (1), in conjunction with Eqn (2), solves simultaneously for E, ψ_T, and ψ_L as functions of plant traits and boundary conditions in the atmosphere (D) and in the soil (ψ_S). The soil water potential is related to the relative soil moisture s through the soil water retention curve $\psi_S = \psi_{S,sat}s^{-b}$ (Clapp & Hornberger, 1978). The effects of the species-specific hydraulic traits (Table S3) on soil moisture trajectories are captured through a transpiration–soil moisture curve (Fig. 1b, solid and dashed lines). A simplified relationship can be obtained by approximating this curve with a piecewise linear function (Fig. 1b, dotted lines). Transpiration E is modeled as a linearly increasing function of s between $s_w < s \le s^*$; there is no transpiration below the wilting point $s_w = s(E = 0.01E_{max})$, and above the incipient stress point $s^* = s(E = 0.85E_{max})$ transpiration is maximized at $E_{max} = 0.95\ \max(E)$, that is,

$$E(s) = \begin{cases} 0 & 0 < s \le s_w \\ E_{max}\frac{s - s_w}{s^* - s_w} & s_w < s \le s^* \\ E_{max} & s^* < s \le s_1 \end{cases}. \quad (3)$$

Equation (3) will be later used to drive a soil moisture balance model.

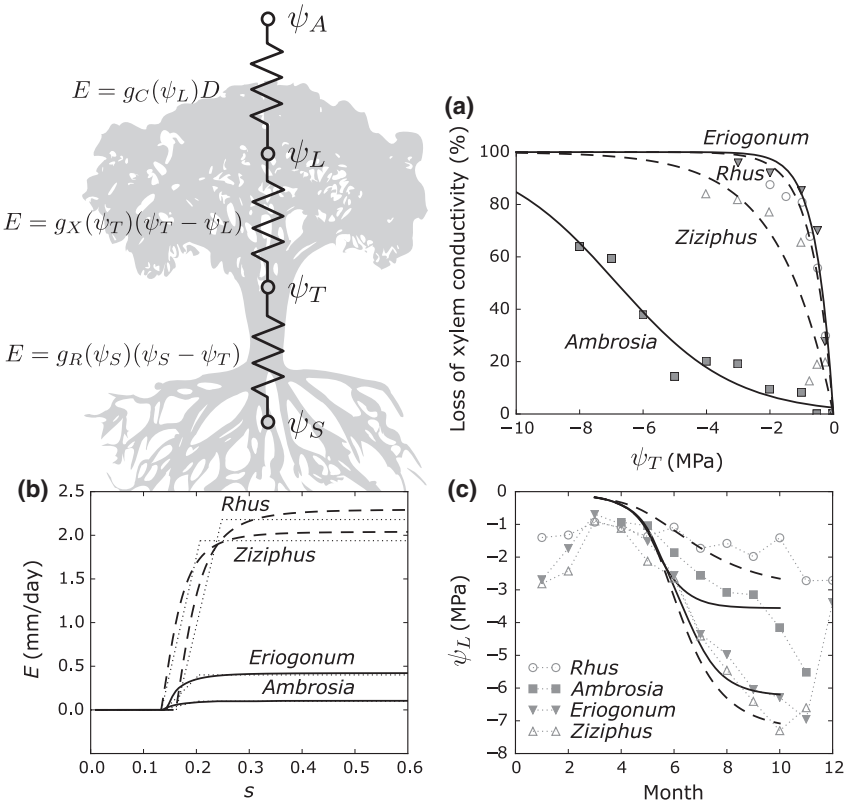

Fig. 1 Measured and modeled species' responses to seasonal drought. The diagram illustrates water flow through a plant, where $\psi_S, \psi_T, \psi_L, \psi_A$ represent water potentials in the soil, stem, leaf, and atmosphere, and the plant transpiration flux (E) is regulated at the soil–root interface, the stem, and the canopy by state-dependent conductivities (g_R, g_X, g_C). D is the vapor pressure deficit. (a) Vulnerability curves for *Rhus ovata* and *Ziziphus parryi* ('profligate water users') are shown with dashed lines, while *Ambrosia salsola* and *Eriogonum fasciculatum* ('conservative water users') are shown in solid lines. (b) Derived relationship of transpiration vs. soil moisture (s) for *Rhus* and *Ziziphus* (dashed lines), and *Ambrosia* and *Eriogonum* (solid lines). The dotted lines show linear approximations. (c) Fitted (lines) and measured (markers) leaf water potentials.

Parameterizing the plant hydraulics model with measured and derived traits

Traits used to parameterize the plant hydraulics model are listed in Table S3 for four representative species: *Ambrosia salsola*, *Eriogonum fasciculatum*, *Rhus ovata*, and *Ziziphus parryi* (hereafter referred to by genus names only). The maximum conductivities in the canopy, the stem, and the soil–root interface in Eqn (2), or $g_{C,max}$, $g_{X,max}$, $g_{R,max}$, are upscaled from measurements at the tissue level and are defined as (Manzoni *et al.*, 2014),

$$g_{C,max} = \frac{g_{C,max,leaf} M_w T_d A_{canopy}}{\rho_w},$$
$$g_{X,max} = \frac{\varepsilon k_{sap} T_d A_{stem}}{L_{stem} \rho_w}, \quad (4)$$
$$g_{R,max} = \frac{v K_{S,sat}}{\rho_w g} \sqrt{\frac{A_{root}}{d_R Z_r}}.$$

The sapwood area-specific hydraulic conductivity in the stem k_{sap} (kg m^{-1} s^{-1} MPa^{-1}), leaf area-specific maximum stomatal conductance $g_{C,max,leaf}$ (mol m^2 s^{-1}), and the leaf area-to-sapwood area ratio LA : SA (m^2 m^{-2}) are measured on each species at the tissue level (Pivovaroff *et al.*, 2016). Sapwood area at the plant-level A_{stem} (m^2 m^{-2}) is calculated from diameter at breast height (DBH, cm) based on an allometric relationship derived for *Quercus suber* in a Mediterranean-type climate, where $A_{stem} = 0.1624\text{DBH}^{1.1822}$ (Caldeira *et al.*, 2015). The canopy area A_{canopy} (m^2 m^{-2}) is the product of A_{stem} and LA : SA, and multiplied by a scaling factor of 2 to upscale tissue level LA : SA to the plant level. Traits shared between all species are the mean canopy height L_{stem} = 1.5 m, root area index A_{root} = 5.5 m^2 m^{-2}, and fine root diameter d_R = 0.5 mm, as well as the saturated soil hydraulic conductivity $K_{s,sat}$ = 1.0 m day^{-1}. Other constants are as follows: $M_w = 0.018$ kg mol^{-1} is the molecular weight of water, $T_d = 36\,000$ s day^{-1} is the transpiration period in a day, $\rho_w = 1000$ kg m^{-3} is the density of water, $\varepsilon = 500$ is an upscaling constant from xylem to stem-level conductivity, $v = 10^6$ Pa MPa^{-1} is a unit conversion factor, and $g = 9.81$ m s^{-2} is the gravitational acceleration constant.

Both the mean rooting depth for each species Z_r (m) and the point of stomatal closure $\psi_{L,0}$ (MPa) are derived from fitting

modeled seasonal leaf water potentials ψ_L in the dry season to measured values (Fig. 1c). During the calibration process, the rooting depth is increased at 0.1 m increments between 0.0 and 1.0 m and at 0.25 m increments between 1.0 and 5.0 m, while the stomatal closure point is assumed to be around the minimum observed seasonal leaf water potential $\psi_{L,min}$, with $\psi_{L,0} = \psi_{L,min}/c$ and c varied from 0.8 to 1.2 in 0.1 increments. The values of Z_r and $\psi_{L,0}$ that gave the best fit (through least square errors) are shown in Table S3 along with other plant hydraulic traits.

parameters relevant to transpiration in Eqn (3) are assumed to apply at the biome level, designated by $s_{w,b}$, s_b^*, $E_{max,b}$, and $Z_{r,b}$ (Table S2). The stochastic steady-state probability density function (PDF) of soil moisture $p(s)$ can then be found analytically for the whole biome (Manzoni *et al*., 2014). The expectation of this PDF (denoted by brackets) is

$$\langle s_{wet}\rangle = h(\lambda_w) = \frac{C}{\eta_b\beta^2}\left(e^{-s_b^*\beta}\left(1+s_b^*\beta\right) - e^{-s_1\beta}(1+s_1\beta)\right) + C\frac{\kappa}{\lambda_w\gamma_b}\left(\frac{\eta_b}{\gamma_b}\right)^{\kappa} e^{-s_{w,b}\gamma_b}\left(s_{w,b}\gamma_b\Gamma\left(\kappa,0,\kappa\frac{\eta_b\gamma_b}{\lambda_w}\right) + \Gamma\left(1+\kappa,0,\kappa\frac{\eta_b\gamma_b}{\lambda_w}\right)\right), \quad (5)$$

Defining hydraulic failure based on seasonal soil moisture dynamics

Coupling the plant response in E, ψ_T, and ψ_L in Eqns (1) and (2) to soil moisture through the water retention curve enables us to find the soil moisture value $s_{\psi 90}$ corresponding to critical plant dehydration thresholds. We designate 90% loss in xylem conductivity as a proxy for hydraulic failure in each species. We have selected this high threshold in the absence of further knowledge on species-specific linkages between xylem conductivity loss and physiological damage. The feedback of plant traits on soil moisture is encapsulated in the three parameters in Eqn (3): the maximum transpiration E_{max} under well-watered conditions, the soil moisture at stress-onset s^* (at which stomatal closure is initiated), and the soil moisture at complete stomatal closure s_w (Table S3). These parameters are inserted into a stochastic soil moisture model, and the resulting mean soil moisture trajectories are used to analyze the probability of crossing specified soil moisture thresholds that relate to plant physiological states.

In seasonally varying environments, whether soil moisture trajectories will cross the critical hydraulic threshold $s_{\psi 90}$ at the end of the dry season depends on its rate of decay during the dry season as well as its initial value, which is determined by wet season soil water recharge. The soil water balance at the daily timescale is determined by stochastic rainfall inputs and deterministic losses from transpiration, drainage, and runoff. Within each season, rainfall is assumed to be described by a stationary marked Poisson process for which the times between rainfall events are drawn from an exponential distribution with mean $1/\lambda_s$, and the depths of rainfall events are drawn independently from another exponential distribution with mean α_s (Rodriguez-Iturbe & Porporato, 2004), where the subscript s can stand for either w in the wet or d in the dry season. Detailed descriptions of the generalized soil moisture model are found in Supporting Information.

During the wet winter season in a Mediterranean-type climate (during which most of the annual rainfall occurs), soil moisture is assumed to quickly reach stochastic steady state (Viola *et al*., 2008). Due to the elevated hydrological response that dominates over the biological response, the

and

$$C = \left(e^{-s_{w,b}\gamma_b}\frac{\kappa}{\lambda_w}\left(\frac{\eta_b}{\gamma_b}\right)^{\kappa}\Gamma\left(\kappa,0,\kappa\frac{\eta_b\gamma_b}{\lambda_w}\right) - \frac{e^{-s_1\beta}-e^{-s_b^*\beta}}{\eta_b\beta}\right)^{-1},$$

where $\eta_b = E_{max,b}/(nZ_{r,b})$, $\gamma_b = nZ_{r,b}/\alpha_w$, λ_w, and α_w are the mean rainfall frequency and depth in the wet season, C is the normalizing constant obtained by imposing $\int_{s_{w,b}}^{s_1} p(s)ds = 1$, β, and κ are nondimensional groups where $\beta = \gamma_b - \lambda_w/\eta_b$ and $\kappa = \lambda_w/\eta_b(s_b^* - s_{w,b})$, and $\Gamma(\cdot,c,d)$ is a generalized incomplete gamma function with integration limits $[c, d]$. The dependence of $\langle s_{wet}\rangle$ on the mean rainfall frequency λ_w is shown in Fig. 2a.

During the dry summer season, soil moisture decays over time from an initial value. Here, we will use the crossing of mean soil moisture $\langle s\rangle$ as proxy for the mean crossing of stochastic soil moisture trajectories, even while acknowledging that they are not exactly the same (Rodriguez-Iturbe & Porporato, 2004, Chapter 3). By averaging the soil water balance (Eqn S1), we have an approximation describing the time course of mean soil moisture $\langle s\rangle$ over the dry season (Laio *et al*., 2002; Feng *et al*., 2015), where the effect of the minimal runoff losses is assumed to be negligible for determining the mean soil moisture trajectory,

$$\frac{d\langle s\rangle}{dt} = \begin{cases} \frac{\lambda_d}{\gamma} - \eta\frac{\langle s\rangle - s_w}{s^* - s_w} & s_w < \langle s\rangle \le s^* \\ \frac{\lambda_d}{\gamma} - \eta & s^* < \langle s\rangle \le s_1 \end{cases}, \quad (6)$$

where $\eta = E_{max}/(nZ_r)$, $\gamma = nZ_r/\alpha_d$, and λ_d and α_d are the mean rainfall frequency and intensity during the dry season. The mean soil moisture during the wet season $\langle s_{wet}\rangle$ (Eqn 5) serves as the initial value for Eqn (6) (Fig. 2b). Unlike during the wet season, however, dry season soil moisture dynamics are now dominated by vegetation feedback, and thus, the transpiration parameters (s_w, s^*, E_{max}, and Z_r) are now specific to each species (Table S3). The stem water potentials corresponding to the soil moisture values reached at the end of the dry season $\langle s(t_d)\rangle$ are compared to measured values of $\psi_{T,min}$ for species in Fig. S1. These species represent a subset of those in Table S1 that retain functional leaves during the dry season, thus minimizing the effects of intraseasonal changes in plant physiological variables. The code used to generate these trajectories can be found in Supporting Information (Data S1–S6).

The advantage of adopting a macroscopic approximation here is that in contrast to the original stochastic formulation of soil water balance (Eqn S1), the mean soil moisture can be

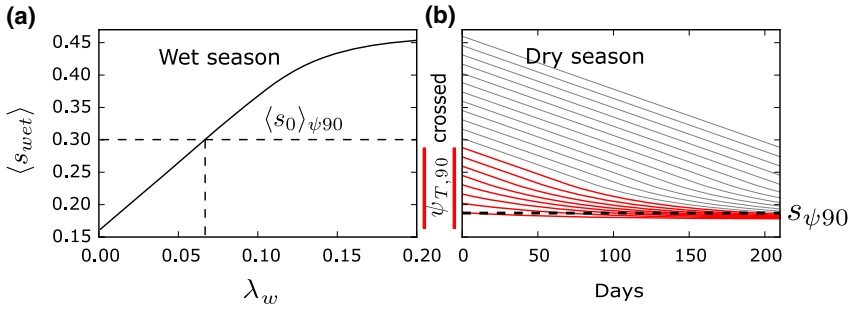

Fig. 2 Schematic of hydraulic threshold crossing based on seasonal soil moisture dynamics. (a) Initial mean soil moisture for the dry season as a function of wet season rainfall frequency λ_w. (b) Mean soil moisture trajectories starting at different initial values over the dry season, parameterized with plant properties for *Rhus* and other soil and climate variables. Red lines correspond to those trajectories that have crossed the soil moisture level leading to hydraulic failure in *Rhus*.

easily resolved in a deterministic manner. Due to the nonlinearity in the transpiration losses (Eqn 3), this macroscopic approximation should only be employed in cases when rainfall amounts are minimal ($(\lambda_d/\gamma) \ll 1$, Laio *et al.*, 2002). During the growing season in Mediterranean-type climates, such a low-rainfall assumption is not unreasonable. In cases where the rainfall during the dry season is high enough to generate substantial runoff and invalidate the macroscopic approximation, an alternate, iterative approach to finding the trajectory of mean soil moisture should be used [e.g., the self-consistent approximation in Feng *et al.* (2015)].

Finally, the initial mean soil moisture value at the beginning of the dry season corresponding to the mean soil moisture $\langle s \rangle$ falling exactly on the hydraulic threshold at the end of the dry season ($\langle s(t_d) \rangle = s_{\psi 90}$) can be solved from Eqn (6) as

$$\langle s_0 \rangle_{\psi 90} = \begin{cases} s_{\psi 90} & s_w < s_{\psi 90} \le s_{tm} \\ \min\left[(s_{\psi 90} - s_{tm}) e^{((\eta t_d)/(s* - s_w))} \right. & \\ \left. + s_{tm}, s^* + \left(\eta - \frac{\lambda_d}{\gamma}\right)(t_d - t_1) \right] & s_{tm} < s_{\psi 90} \le s^* \\ s_{\psi 90} + \left(\eta - \frac{\lambda_d}{\gamma}\right) t_d & s^* < s_{\psi 90} \le s_1 \end{cases}, \tag{7}$$

where $s_{tm} = s_w + (\lambda_d/\gamma\eta)(s^* - s_w)$ and $t_1 = -((s^* - s_w)/\eta) \log((s_{\psi 90} - s_{tm})/(s^* - s_{tm}))$. Due to the monotonic decrease in $\langle s \rangle$ during the dry season, any initial value below $\langle s_0 \rangle_{\psi 90}$ guarantees that the hydraulic threshold will be crossed at the end of the dry season (Fig. 2b). As such, the climatic conditions during the wet season leading to the crossing of the critical hydraulic threshold in the dry season can be related to $\langle s_0 \rangle_{\psi 90}$ by comparison with $\langle s_{wet} \rangle$ (Eqn 5). The crossing of the critical hydraulic threshold can then be cast as a function of the dry and wet season rainfall frequencies, λ_d and λ_w.

Analysis of observed species distributions

To test the practicality of the model results, observations of *Rhus* ($n = 1019$, a 'profligate' water user) and *Eriogonum* ($n = 1798$, a 'conservative' water user) within California are obtained from the Consortium of California Herbaria (http://ucjeps.berkeley.edu/consortium/) and correlated with their associated long-term average precipitation in the late summer (July–September) and late winter (December–March). Each observation for *Rhus* or *Eriogonum* is paired with precipitation data from a nearby station within 40 kilometers, drawn from the NOAA Cooperative Stations network (and accessed from the Western Regional Climate Center website; www.wrcc.dri.edu/climatedata/climsum/). The seasonal precipitation values associated with each species' observation is fitted with gamma distributions, and Mann–Whitney *U*-tests are used to see whether species observations are likely to be associated with distinctly different winter and summer precipitation profiles.

Plant hydraulic risk and sensitivities to seasonal rainfall

Differences in their responses to seasonal rainfall notwithstanding, the largest source of uncertainty about plant water availability and hydraulic risk in the Southern California study region comes from interannual variability in rainfall. The large-scale circulation patterns that control seasonal rainfall are characterized by variability at the interannual and interdecadal timescales; as such, rainfall variability is thought to reach a 'local' equilibrium within each year, described by statistics that nevertheless fluctuate over longer timescales (Porporato *et al.*, 2006). Mathematically, this means that the long-term variability in the seasonal rainfall statistics can be modeled by PDFs. The variables of particular interest are the wet and dry season rainfall frequencies, λ_w and λ_d. We now consider the seasonal rainfall frequencies λ_d and λ_w as random variables, independently varying on an annual basis, and describe their observed long-term distributions from a nearby weather station using two gamma distributions, $f_w(\lambda)$ and $f_d(\lambda)$ (Table S2). The risk of the soil moisture crossing $s_{\psi 90}$ is then modulated by the probability of specific values of λ_d and λ_w being realized in any given year, or:

$$Q = \int_{\lambda_d' \in \lambda_d} F_w(h^{-1}(\langle s_0 \rangle_{\psi 90} | \lambda_d')) f_d(\lambda_d') d\lambda_d', \tag{8}$$

where the function $h^{-1}(\cdot)$ gives the maximum wet season rainfall frequency λ_w that ensures crossing of $s_{\psi 90}$ from an initial condition $\langle s_0 \rangle_{\psi 90}$ [inverse of Eqn (5) when set to (7)], and $F_w(\lambda)$

is the cumulative density function of $f_w(\lambda)$ that gives the probability of observing a particular value of λ_w or below. Together, $F_w(h^{-1}(\langle s_0\rangle_{\psi 90}))$ gives the probability of crossing $s_{\psi 90}$ based on the interannual variability of λ_w. The interannual variability in λ_d is incorporated by conditioning the previous crossing term $h^{-1}(\langle s_0\rangle_{\psi 90})$ on dry season rainfall frequency, and integrating over possible values of λ_d in its long-term distribution $f_d(\lambda)$. Thus, the risk metric in Eqn (8) gives the probability of crossing a hydraulic threshold in a given year based on species characteristics, soil properties, and seasonal climatic conditions, and weights that probability by the likelihood of realizing those climatic conditions independently in any given year, assuming that their occurrence is described by stationary PDFs. Similarly, the expected seasonal transpiration for each species is derived as

$$\langle \mathrm{ET}_{\mathrm{seas}}\rangle = \int_{\lambda'_d\in\lambda_d}\int_{\lambda'_w\in\lambda_w} \mathrm{ET}_{\mathrm{seas}}(\lambda'_w,\lambda'_d) f_w(\lambda'_w) f_d(\lambda'_d)\mathrm{d}\lambda'_w\mathrm{d}\lambda'_d, \quad (9)$$

based on the expected values of the cumulative growing season transpiration [from Eqns (3) and (6)] integrated over possible values of λ_w and λ_d over many years. The integration is performed through Monte Carlo integration over $f_w(\lambda)$ and $f_d(\lambda)$.

We used this framework to examine the sensitivity of different species to potential changes in seasonal rainfall statistics through their risks of hydraulic failure Q and their expected seasonal transpiration $\langle \mathrm{ET}_{\mathrm{seas}}\rangle$. This is performed by varying the shape χ and scale θ parameters of the gamma distributions $f_w(\lambda)$ and $f_d(\lambda)$ in a way to maintain constant variances for $f_w(\lambda)$ and $f_d(\lambda)$ while shifting their means. *Rhus* and *Eriogonum* were again used as illustrative cases of species with divergent responses to a common imposed change. We studied the most likely future rainfall scenario for this region, in which winter rainfall frequency decreases but summer rainfall frequency increases relative to the current climate (Pierce *et al.*, 2013).

Results

Plant hydraulic status cannot be deduced from water use

The coupled soil–plant model effectively differentiated species based on their water status at the end of the summer (see Fig. S1 for predicted and measured values of $\psi_{T,\min}$). Four species, spanning a broad range of water-use patterns and physiological strategies, illustrate these results in Fig. 3: *A. salsola*, *E. fasciculatum*, *R. ovata*, and *Z. parryi*. 'Profligate' water users (*Ziziphus* and *Rhus*, dashed lines) are separated from 'conservative' water users (*Eriogonum* and *Ambrosia*, solid lines), based on their transpiration rates (Fig. 3c; Pivovaroff *et al.*, 2016). Moreover, these water-use strategies are shown to be independent of measured water status and seasonal water stress (Fig. 3b, c).

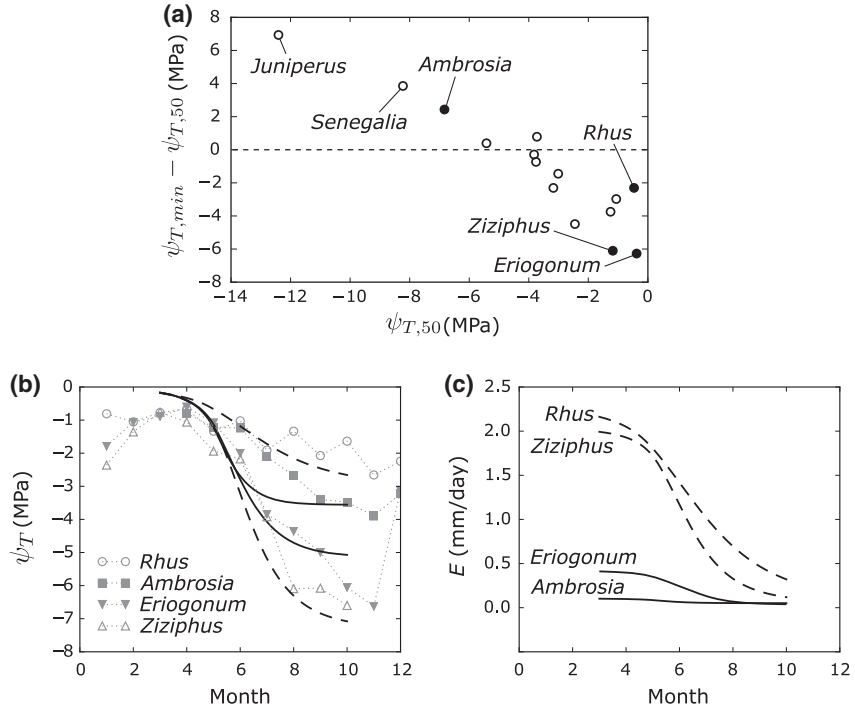

Fig. 3 Measured and modeled species' responses to seasonal drought. (a) Observed seasonal hydraulic safety margins ($\psi_{T,\min} - \psi_{T,50}$) vs. cavitation resistance ($\psi_{T,50}$) for 15 species from a Mediterranean chaparral–desert ecotone (Table S1). (b) Modeled and measured stem water potentials (ψ_T) of *Rhus ovata* and *Ziziphus parryi* (profligate water users, in dashed lines), and *Ambrosia salsola* and *Eriogonum fasciculatum* (conservative water users, in solid lines). (c) Modeled transpiration (E) for those same species over the dry season.

The divergence between plant water use and water stress for species in Fig. 3 demonstrates that similar water flux patterns can arise from different hydraulic pathways. For example, *Ziziphus* and *Rhus* are both deep-rooted species that transpire profusely during the dry season, and are thus considered 'profligate' water users (Pivovaroff *et al.*, 2016). However, because *Rhus* has a much lower xylem cavitation resistance (less negative $\psi_{T,50}$, Table S3) and greater stomatal regulation (less negative $\psi_{L,0}$), it experiences a more moderate decay in its leaf and stem water potentials relative to *Ziziphus* (Fig. 3b). Similarly, *Eriogonum* and *Ambrosia* are both 'conservative' water users with lower transpiration rates and draw water from shallower soils, but *Eriogonum* experiences a much steeper seasonal decay in its leaf and stem water potentials compared to *Ambrosia* (Fig. 3b). This could be attributed to *Eriogonum*'s lower cavitation resistance (but not to greater stomatal regulation, as $\psi_{L,0}$ for *Eriogonum* is more negative than that of *Ambrosia*, Table S3) and possibly to its higher leaf area-to-sapwood area ratio, which allows the xylem to more 'efficiently' supply water to the leaves at greater risk of cavitation (Tyree *et al.*, 1994). While it is useful to classify these species into functional categories based on their water-use amounts (especially for the purpose of accounting for surface water fluxes), or into categories associated with their tendency to adjust plant water potentials (isohydry/anisohydry, Martinez-Vilalta *et al.*, 2014; Meinzer *et al.*, 2016), it is also evident that embedded within the same categories lies a range of traits that results in divergent outcomes in terms of plant water status or plant fluxes. The results provoke the question of whether new axes of functional variation are required to complement existing classifications along the conservative/opportunistic (Rodriguez-Iturbe *et al.*, 2001) or isohydric/anisohydric axes, even as the use of these classifications as suitable indicators of drought vulnerability are

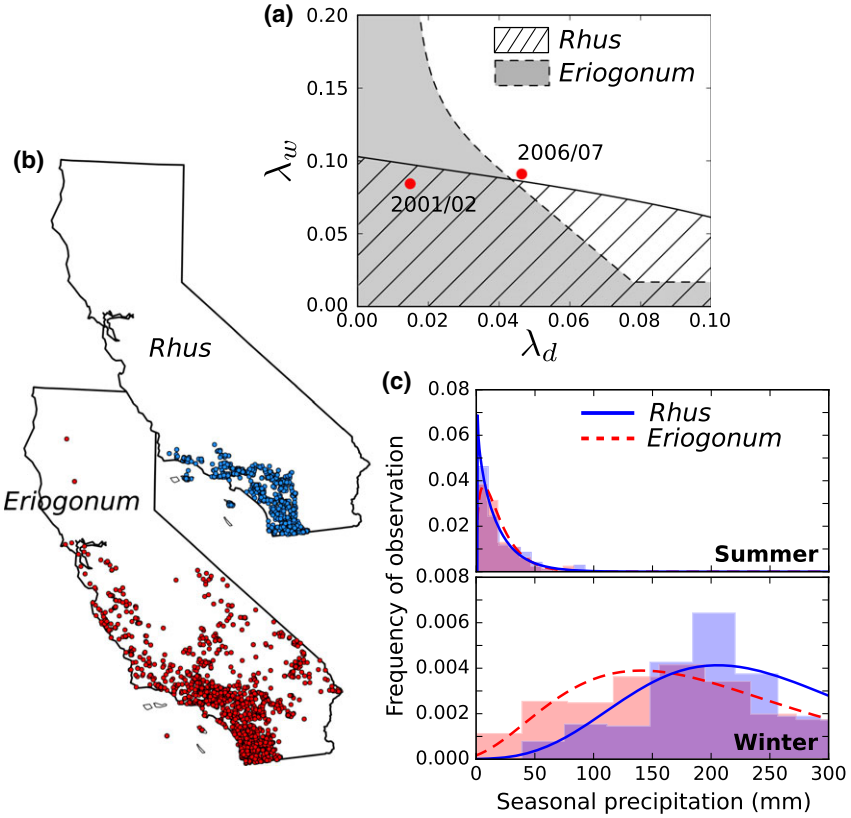

Fig. 4 Dependence of hydraulic threshold crossings on seasonality of rainfall. (a) Predicted zones of hydraulic failure for *Rhus* (hatched) and *Eriogonum* (shaded), based on wet and dry season rainfall frequencies, λ_w and λ_d, and a dry season vapor pressure deficit of 2.0 kPa. The red dots correspond to notable years when mortality was observed for one or both species. (b) Observed instances of *Rhus* and *Eriogonum* across California. (c) Frequency of observations for *Rhus* (solid blue lines) and *Eriogonum* (dashed red lines) in California that correspond to long-term late summer (July–September, top panel) and late winter (December to March, bottom panel) precipitation. Mann–Whitney *U*-tests reject the null hypothesis that the *Rhus* and *Eriogonum* observations are associated with the same winter precipitation distribution (*P*-value $\ll$ 0.01) but cannot do so for their summer precipitation distributions (*P*-value = 0.234).

subjected to deliberation (Martínez-Vilalta & Garcia-Forner, 2016).

Differences in seasonal hydraulic risk, drought susceptibility, and habitat extent align

The dependence of hydraulic failure on the seasonal rainfall statistics is shown in Fig. 4a for *Rhus* and *Eriogonum*. These species have the lowest cavitation resistance (least negative $\psi_{T,50}$) and the most recorded instances of mortality/dieback among the studied species in the area. The hatched and shaded areas in Fig. 4a show where our model predicts mean soil moisture would cross the critical hydraulic threshold for each species ($s_{\psi 90}$) by the end of the dry season, based on rainfall frequencies in the dry season (λ_d) and wet season (λ_w). The results suggest that the confluence of hydraulic traits for *Rhus* (including deeper roots, lower maximum transpiration rate, and earlier stomatal closing) allowed it to subsist through dry summers by relying more on winter soil recharge. *Eriogonum*, in comparison, can be more vulnerable during dry summers due to its reliance on summer rainfall. Other species predicted to cross their respective hydraulic thresholds in the study region are *Z. parryi* and *Quercus cornelius-mulleri* (Fig. S2), also among those with the lowest cavitation resistance.

Due to the existence of uncertainties in the model – from parameters inputs and model structure – as well as limitations of the data used for validation, we have based our analysis not on the absolute values of the results but on the relative comparison across species. We offer two such qualitative corroborations for *Rhus* and *Eriogonum* based on limited empirical data. First, *Rhus* and *Eriogonum* have been observed to sustain different degrees of mortality/dieback during shared drought events in this region, and this difference is amplified when summer rainfall is anomalously low. For example, *Rhus* and *Eriogonum*, respectively, suffered 24% and 71% loss in cover through dieback during the dry period in 2006/2007 at the study site in Morongo Valley, California (red points, Fig. 4a). Additionally, following an extremely dry summer in 2002, the *Eriogonum* population virtually perished (with 95% mortality rate) at a nearby site in Joshua Tree National Park (32 km from Morongo Valley; Miriti *et al.*, 2007). During the same period, the *Rhus* population at a location near Pinyon Pines, California, 64 kilometres from Morongo Valley, suffered only moderate dieback (scoring 2, indicating minor dead foliage, of 5; Paddock *et al.*, 2013). These observations indicate that *Eriogonum* tend to be more adversely affected during low summer rainfall years than *Rhus*.

Second, the spatial distributions of *Rhus* and *Eriogonum* are consistent with their inferred dependence on winter and summer rainfall. *Rhus* is mostly found within the California Floristic Province, which is dominated by winter rainfall, while *Eriogonum* is also distributed in Nevada and Utah and more broadly in Arizona, in desert-like areas where summer rainfall can be more important for many plants in this region (USDA PLANTS Database, http://plants.usda.gov/). We also correlated observations of *Rhus* and *Eriogonum* within California to their corresponding winter or summer rainfall (Fig. 4b, c) and found that *Rhus* is much more likely to be found in areas with higher winter rainfall compared to *Eriogonum*.

Plant traits generate divergent sensitivities to climate change

The sensitivities of *Rhus* and *Eriogonum* to seasonal rainfall can be examined by quantifying their probabilities of crossing their respective critical hydraulic threshold $s_{\psi 90}$ over a range of seasonal rainfall frequencies. We have done so by varying the shape χ and scale θ parameters of the gamma distributions for wet and dry season rainfall frequencies, $f_w(\lambda)$ and $f_d(\lambda)$ (Table S2), and rescaling their means from 0.5 to 1.5 times their present values, representing a 50% decrease to a 150% increase in the mean rainfall frequency in the two seasons. The results indicate divergent effects of projected climate change on water stresses and seasonal transpiration experienced by *Rhus* and *Eriogonum*. Under the current climate (arrow origins, Fig. 5), the risks of *Rhus* and *Eriogonum* crossing the 90% conductivity loss threshold are comparable (Fig. 5c, d). However, under the most likely future rainfall scenario (arrow tips), *Eriogonum* is predicted to experience a minor reduction in the likelihood of crossing this threshold, while *Rhus* is predicted to experience an increased likelihood. These diverging sensitivities can be attributed to *Rhus*'s greater reliance on winter rainfall compared to *Eriogonum*, which is more sensitive to changes in summer rainfall (Fig. 4a). On the other hand, the mean seasonal transpiration for both *Rhus* and *Eriogonum* is expected to change little (<1%) in response to changes in rainfall frequencies (Fig. 5a, b). The direction of change in mean seasonal transpiration for each species is, somewhat counterintuitively, correlated with that of hydraulic risk, leading to scenarios in which a species' seasonal transpiration and hydraulic risk can simultaneously increase (for *Rhus*) or decrease (for *Eriogonum*).

Finally, a Sobol's global sensitivity analysis (Sobol, 2001; Fig. S3) reveals that hydraulic risk and seasonal transpiration are differently influenced by plant traits: hydraulic risk Q was most sensitive to uncertainty in

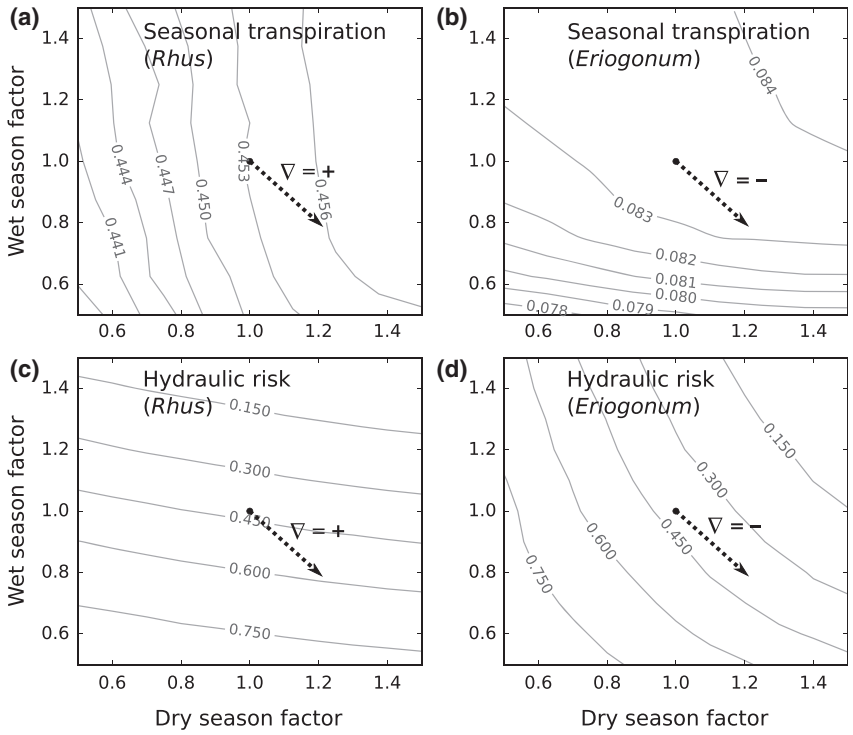

Fig. 5 Changes in mean seasonal transpirations $\langle ET_{seas} \rangle$ [m; Eqn (9)] as a function of changes in the mean of the probability density functions for rainfall frequency in the wet or the dry seasons, $f_w(\lambda)$ and $f_d(\lambda)$, from 0.5 to 1.5 times their present values (represented by wet and dry season factors) for (a) *Rhus* and (b) *Eriogonum*. Changes in hydraulic risks Q [Eqn (8)] under the same schemes are shown for *Rhus* and *Eriogonum* in (c) and (d). The origins of the arrows indicate current climate conditions; the tips indicate projected future conditions.

the stomatal closure point ($\psi_{L,0}$) and the stem vulnerability parameters (a and $\psi_{T,50}$), while mean seasonal transpiration $\langle ET_{seas} \rangle$ was most sensitive to uncertainty in the size of the canopy (A_{canopy}) and rooting depth (Z_r). These analyses underscore the importance for basing ecohydrological predictions on an understanding of the trait-based, hydrodynamic origins of plant water status and water flux.

Discussion

The dichotomous focus on resolving either the internal plant water status or external hydraulic flux can be reconciled by recognizing their underlying hydrodynamic connections through the plant hydraulic system (Cruiziat *et al*., 2002). Parameterizing a parsimonious model with a set of species-specific physiological, morphological, and behavioral traits, we showed that the aggregated effect of these traits can result in independently divergent outcomes in plant water status and plant water flux. In other words, the pathways to drought survival are not always defined through the same traits, nor are they always correlated with transpiration rates; 'conservative' water users – those with minimal water flux – can experience seasonal drops in their water potential that are as steep as those of 'profligate' water users (Fig. 3). Thus, adopting either hydraulic status or flux as a sole guidepost for drought response prediction is likely to be problematic – the two measures are nonreciprocal, have contrasting sensitivities to parameter uncertainties during model calibration, and both must be considered in order to describe the long-term relationships between community composition and ecosystem function (Adams *et al*., 2012). Our model provides a simple but useful route toward resolving these difficulties.

The model predicts species-level differences in their vulnerability to low seasonal rainfall that are consistent with observed drought-induced dieback at the local scale as well as species distributions at the regional scale. By interrogating the model through changes in seasonal rainfall statistics, we showed that the projected climate in Southern California will likely shift favorability of survival from one representative species to another. This demonstrates how differences in the intrinsic sensitivities of species within the same community can become a key determinant of ecosystem change (Cornwell *et al*., 2012), providing insight into potential effects of future climate scenarios on community composition.

Although applied to Southern California, our approach is generalizable to other climates and biomes,

provided that there are suitably comprehensive physiological data to describe the suite of plant hydraulic traits and water-use strategies. We note that such data, particularly across a plant community, remain relatively scarce. As a result, there are other physiological and behavioral features that are not captured within the model, much less measured as a part of a comprehensive dataset, that could exacerbate or alleviate the drought response in each species. The present modeling framework excludes the roles of incomplete xylem refilling over multiple dry down cycles, vertical distribution of roots, phenological adjustments in leaf area, sapwood area, or root area in response to drought over time, and other transient or hysteretic effects that would rule out a one-to-one correspondence between internal hydraulic status and external soil moisture conditions. Despite these omissions, the simplicity of the model enables parameterization primarily with empirical data, in contrast to models that have relied to a greater extent on calibration or assumptions in the absence of measurements or on the use of effective parameters (Parolari *et al*., 2014; Mackay *et al*., 2015). It has also allowed us to show for the first time the salient connection between physiologically meaningful hydraulic traits and species-level sensitivities to nuanced changes in the climate, especially at the seasonal scale.

The modeling work presented here offers a parsimonious approach to the joint exploration of water cycling and drought-induced mortality risk, yet additional refinements would be needed before adopting it as a predictive framework. Most importantly, stored nonstructural carbohydrates are thought to convey drought resistance to plants (O'Brien *et al*., 2014) by contributing to cell turgor maintenance, xylem development, and embolism repair (Nardini *et al*., 2011; Deslauriers *et al*., 2016), and a proper accounting of the carbon balance and its interaction with hydraulic processes within the plant will better reflect its role in mitigating the most extreme effects of drought. Other refinements include the effects of species interactions on their common moisture environment (Gilman *et al*., 2010), improved representations of hydrology including the effects of topography (Thompson *et al*., 2011), and belowground processes such as hydraulic redistribution (Hultine *et al*., 2003) or access to groundwater or surface water sources (Miller *et al*., 2010) as well as the geologic history of the soil (Hamerlynck & McAuliffe, 2008) that alter the resources available to different individuals across the landscape. Our approach has singled out key parameters that can capture a range of water-use strategies and a hydraulic risk framework that is responsive to a considerable level of temporal complexity in a hierarchy of rainfall variabilities over homogeneous terrain. It presents a promising interface for bridging the prediction of hydraulic risk, modulated by soil moisture and plant feedbacks, into more spatially explicit ecosystem models.

Acknowledgements

X. F. was supported by the NOAA Climate and Global Change Postdoctoral Fellowship. S. E. T., D. D. A., and T. E. D. thank the NSF for supporting RAPID grant IOS 1441396. L. S. S. was supported by NSF grant 0817212 and 1548846 as well as Bureau of Land Management Project #61328. The authors would also like to thank William R. L. Anderegg and three anonymous reviewers for providing valuable feedback and suggestions.

References

Adams HD, Luce CH, Breshears DD *et al*. (2012) Ecohydrological consequences of drought- and infestation-triggered tree die-off: insights and hypotheses. *Ecohydrology*, **5**, 145–159.

Anderegg WRL, Klein T, Bartlett M, Sack L, Pellegrini AFA, Choat B (2016) Meta-analysis reveals that hydraulic traits explain cross-species patterns of drought-induced tree mortality across the globe. *Proceedings of the National Academy of Sciences USA*, **113**, 2–7.

Araujo M, Peterson AT (2012) Uses and misuses of bioclimatic envelope modeling. *Ecology*, **93**, 1527–1539.

Barigah TS, Charrier O, Douris M *et al*. (2013) Water stress-induced xylem hydraulic failure is a causal factor of tree mortality in beech and poplar. *Annals of Botany*, **112**, 1431–1437.

Breshears DD, Myers OB, Meyer CW *et al*. (2009) Tree die-off in response to global change-type drought: mortality insights from a decade of plant water potential measurements. *Frontiers in Ecology and the Environment*, **7**, 185–189.

Caldeira MC, Lecomte X, David TS, Pinto JG, Bugalho MN, Werner C (2015) Synergy of extreme drought and shrub invasion reduce ecosystem functioning and resilience in water- limited climates. *Scientific Reports*, **5**, 15110.

Choat B, Jansen S, Brodribb TJ *et al*. (2012) Global convergence in the vulnerability of forests to drought. *Nature*, **491**, 752–755.

Clapp RB, Hornberger GM (1978) Empirical equations for some soil hydraulic properties. *Water Resources Research*, **14**, 601–604.

Cornwell WK, Stuart S, Ramirez A, Dolanc CR, Thorne JH, Ackerly DD (2012) Climate change impacts on California vegetation: physiology, life history, and ecosystem change. California Energy Commission. Publication number: CEC-500-2012-023.

Cruiziat P, Cochard H, Ameglio T (2002) Hydraulic architecture of trees: main concepts and results. *Annals of Forest Science*, **59**, 723–752.

Deslauriers A, Huang J-G, Balducci L, Beaulieu M, Rossi S (2016) The contribution of carbon and water in modulating wood formation in black spruce saplings. *Plant Physiology*, **170**, 2072–2084.

Eamus D (1999) Ecophysiological traits of deciduous and evergreen woody species in the seasonally dry tropics. *Trends in Ecology and Evolution*, **14**, 11–16.

Feng X, Porporato A, Rodriguez-Iturbe I (2015) Stochastic soil water balance under seasonal climates. *Proceedings of the Royal Society of London A: Mathematical, Physical and Engineering Sciences*, **471**, 20140623.

Galbraith D, Levy PE, Sitch S, Huntingford C, Cox P, Williams M, Meir P (2010) Multiple mechanisms of Amazonian forest biomass losses in three dynamic global vegetation models under climate change. *New Phytologist*, **187**, 647–665.

Gilman SE, Urban MC, Tewksbury J, Gilchrist GW, Holt RD (2010) A framework for community interactions under climate change. *Trends in Ecology and Evolution*, **25**, 325–331.

Hamerlynck EP, McAuliffe JR (2008) Soil-dependent canopy die-back and plant mortality in two Mojave Desert shrubs. *Journal of Arid Environments*, **72**, 1793–1802.

Hawkins E, Sutton R (2011) The potential to narrow uncertainty in projections of regional precipitation change. *Climate Dynamics*, **37**, 407–418.

Hultine KR, Cable WL, Burgess SSO, Williams DG (2003) Hydraulic redistribution by deep roots of a Chihuahuan Desert phreatophyte. *Tree Physiology*, **23**, 353–360.

Katul G, Porporato A, Oren R (2007) Stochastic dynamics of plant-water interactions. *Annual Review of Ecology, Evolution, and Systematics*, **38**, 767–791.

Knapp AK, Briggs JM, Smith MD (2012) Community stability does not preclude ecosystem sensitivity to chronic resource alteration. *Functional Ecology*, **26**, 1231–1233.

Laio F, Porporato A, Ridol L, Rodriguez-iturbe I (2001) Plants in water-controlled ecosystems: active role in hydrologic processes and response to water stress II. Probabilistic soil moisture dynamics. *Advances in Water Resources*, **24**, 707–723.

Laio F, Porporato A, Ridolfi L, Rodriguez-Iturbe I (2002) On the seasonal dynamics of mean soil moisture. *Journal of Geophysical Research*, **107**, 1–9.

Mackay DS, Roberts DE, Ewers BE, Sperry JS, McDowell NG, Pockman WT (2015) Interdependence of chronic hydraulic dysfunction and canopy processes can improve integrated models of tree response to drought. *Water Resources Research*, **51**, 6156–6176.

Manzoni S, Vico G, Porporato A, Katul G (2013) Biological constraints on water transport in the soil-plant-atmosphere system. *Advances in Water Resources*, **51**, 292–304.

Manzoni S, Vico G, Katul G, Palmroth S, Porporato A (2014) Optimal plant water-use strategies under stochastic rainfall. *Water Resources Research*, **50**, 1–16.

Martínez-Vilalta J, Garcia-Forner N (2016) Water potential regulation, stomatal behaviour and hydraulic transport under drought: deconstructing the iso/anisohydric concept. *Plant, Cell & Environment*. doi: 10.1111/pce.12846.

Martinez-Vilalta J, Poyatos R, Aguade D, Retana J, Mencuccini M (2014) A new look at water transport regulation in plants. *New Phytologist*, **204**, 105–115.

Meinzer FC, Woodruff DR, Marias DE, Smith DD, McCulloh KA, Howard AR, Magedman AL (2016) Mapping "hydroscapes" along the iso- to anisohydric continuum of stomatal regulation of plant water status. *Ecology Letters*, **19**, 1343–1352.

Menne MJ, Durre I, Vose RS, Gleason BE, Houston TG (2012) An overview of the global historical climatology network-daily database. *Journal of Atmospheric and Oceanic Technology*, **29**, 897–910.

Miller GR, Chen X, Rubin Y, Ma S, Baldocchi DD (2010) Groundwater uptake by woody vegetation in a semiarid oak savanna. *Water Resources Research*, **46**, 1–14.

Miriti MN, Rodriguez-Buritica S, Wright SJ, Howe HF, Rodríguez-Buriticá S, Wright SJ, Howe HF (2007) Episodic death across species of desert shrubs. *Ecology*, **88**, 32–36.

Nardini A, Lo Gullo MA, Salleo S (2011) Refilling embolized xylem conduits: is it a matter of phloem unloading? *Plant Science*, **180**, 604–611.

O'Brien MJ, Leuzinger S, Philipson CD *et al*. (2014) Drought survival of tropical tree seedlings enhanced by non-structural carbohydrate levels. *Nature Climate Change*, **4**, 710–714.

Paddock W, Davis S, Pratt R, Jacobsen A, Tobin M, López-Portillo J, Ewers F (2013) Factors determining mortality of adult chaparral shrubs in an extreme drought year in California. *Aliso*, **31**, 49–57.

Pammenter NW, Willigen CV (1998) A mathematical and statistical analysis of the curves illustrating vulnerability of xylem to cavitation. *Tree Physiology*, **18**, 589–593.

Parolari AJ, Katul GG, Porporato A (2014) An ecohydrological perspective on drought-induced forest mortality. *Journal of Geophysical Research: Biogeosciences*, **119**, 965–981.

Pierce DW, Das T, Cayan DR *et al*. (2013) Probabilistic estimates of future changes in California temperature and precipitation using statistical and dynamical downscaling. *Climate Dynamics*, **40**, 839–856.

Pivovaroff AL, Pasquini SC, De Guzman ME, Alstad KP, Stemke JS, Santiago LS (2016) Multiple strategies for drought survival among woody plant species. *Functional Ecology*, **30**, 517–526.

Porporato A, Vico G, Fay PA (2006) Superstatistics of hydro-climatic fluctuations and interannual ecosystem productivity. *Geophysical Research Letters*, **33**, L15402.

Powell TL, Galbraith DR, Christoffersen BO *et al*. (2013) Confronting model predictions of carbon fluxes with measurements of Amazon forests subjected to experimental drought. *New Phytologist*, **200**, 350–364.

Rodriguez-Iturbe I, Porporato A (2004) *Ecohydrology of Water-Controlled Ecosystems*. Cambridge University Press, Cambridge, UK.

Rodriguez-Iturbe I, Porporato A, Laio F, Ridolfi L (2001) Intensive or extensive use of soil moisture: plant strategies to cope with stochastic water availability. *Geophysical Research Letters*, **28**, 4495–4497.

Sevanto S, Mcdowell NG, Dickman LT, Pangle R, Pockman WT (2014) How do trees die? A test of the hydraulic failure and carbon starvation hypotheses. *Plant, Cell and Environment*, **37**, 153–161.

Sitch S, Huntingford C, Gedney N *et al*. (2008) Evaluation of the terrestrial carbon cycle, future plant geography and climate-carbon cycle feedbacks using five Dynamic Global Vegetation Models (DGVMs). *Global Change Biology*, **14**, 2015–2039.

Skelton RP, West AG, Dawson TE (2015) Predicting plant vulnerability to drought in biodiverse regions using functional traits. *Proceedings of the National Academy of Sciences USA*, **112**, 5744–5749.

Sobol IM (2001) Global sensitivity indices for nonlinear mathematical models and their Monte Carlo estimates. *Mathematics and Computers in Simulation*, **55**, 271–280.

Sperry JS, Adler FR, Campbell GS, Comstock JP (1998) Limitation of plant water use by rhizosphere and xylem conductance: results from a model. *Plant, Cell and Environment*, **21**, 347–359.

Sperry JS, Hacke UG, Oren R, Comstock JP (2002) Water deficits and hydraulic limits to leaf water supply. *Plant, Cell and Environment*, **25**, 251–263.

Tardieu F, Simonneau T (1998) Variability among species of stomatal control under fluctuating soil water status and evaporative demand: modelling isohydric and anisohydric behaviours. *Journal of Experimental Botany*, **49**, 419–432.

Thompson SE, Harman CJ, Troch PA, Brooks PD, Sivapalan M (2011) Spatial scale dependence of ecohydrologically mediated water balance partitioning: a synthesis framework for catchment ecohydrology. *Water Resources Research*, **47**, 1–20.

Tyree M, Ewers F (1991) The hydraulic architecture of trees and other woody plants. *New Phytologist*, **119**, 345–360.

Tyree MT, Davis SD, Cochard H (1994) Biophysical perspectives of xylem evolution: is there a tradeoff of hydraulic efficiency for vulnerability to dysfunction? *IAWA Journal*, **15**, 335–360.

Vico G, Thompson SE, Manzoni S et al. (2015) Climatic, ecophysiological, and phenological controls on plant ecohydrological strategies in seasonally dry ecosystems. *Ecohydrology*, **8**, 660–681.

Viola F, Daly E, Vico G, Cannarozzo M, Porporato A (2008) Transient soil-moisture dynamics and climate change in Mediterranean ecosystems. *Water Resources Research*, **44**, 1–12.

Supporting Information

Additional Supporting Information may be found in the online version of this article:

Figure S1. Comparison of predicted and observed seasonal minimum stem water potential, $\psi_{T,min}$. Species abbreviations are as follows: RHOV, *Rhus ovata*; PUTR, *Purshia tridentata*; QUCO, *Quercus cornelius-mulleri*; AMSA, *Ambrosia salsola*; PSAR, *Psorothamnus arborea*; JUCA, *Juniperus californica*; PRFA, *Prunus fasciculatum*; ERFA, *Eriogonum fasciculatum*; ZIPA, *Ziziphus parryi*.

Figure S2 Predicted zones of hydraulic failure for *Quercus cornelius-mulleri* and *Ziziphus parryi*, based on wet and dry season rainfall frequencies λ_w and λ_d and a dry season vapor pressure deficit of 2.0 kPa.

Figure S3. Sobol's global sensitivity analysis for the predicted risk of crossing the hydraulic failure threshold (top) and mean growing season transpiration (bottom) under current climate conditions.

Table S1. Species names, abbreviations, and measured values of cavitation resistance ($\psi_{T,50}$), minimum stem water potential ($\psi_{T,min}$), and safety margins ($\psi_{T,min} - \psi_{T,50}$).

Table S2. Soil, biome, and climate parameters used in the model, along with their sources.

Table S3. Hydraulic traits and derived parameters for four representative chaparral species (AMSA: *Ambrosia salsola*, ERFA: *Eriogonum fasciculatum*, RHOV: *Rhus ovata*, ZIPA: *Ziziphus parryi*).

Data S1. Traits data for species.

Data S2. Water potential data for species.

Data S3. This file contains a range of functions for importing and processing data from the accompanying excel workbooks, initializing different species, calculating the dry season trajectories for transpiration and water potentials for each species, then consolidating those trajectories onto plots.

Data S4. Contains atmospheric, molecular, and other constants required for initializing the model.

Data S5. Contains hydraulic parameters for different soil types.

Data S6. The class structures for the coupled soil-plant-atmosphere hydrodynamic model.